International Journal of Modern Physics B
2050287 (14 pages)

DOI: 10.1142/S0217979220502872

Flow and thermal management of MHD Cross nanofluids over a thin needle with auto catalysis chemical reactions

Yu-Ming Chu*

Department of Mathematics, Huzhou University, Huzhou 313000, P. R. China

Hunan Provincial Key Laboratory of Mathematical Modeling and Analysis in Engineering, Changsha University of Science and Technology, Changsha 410114, P. R. China
chuyuming@zjhu.edu.cn

M. Ijaz Khan†

Department of Mathematics, Riphah International University, I-14, Islamabad 44000, Pakistan
ijazfmg_khan@yahoo.com

M. Israr Ur Rehman

Department of Mathematics, Quaid-I-Azam University 45320, Islamabad 44000, Pakistan

Seifedine Kadry

Department of Mathematics and Computer Science, Beirut Arab University, Beirut, Lebanon

M. K. Nayak

Department of Physics, IHSE, Siksha "O" Anusandhan Deemed to be University, Bhubaneswar 751003, India

Received 28 June 2020
Revised 23 July 2020
Accepted 28 July 2020
Published 28 October 2020

This research work concerns the investigation of electrically conducting stagnation point flow, heat and mass transport of magneto-Cross nanofluids towards a moving and stretched surface of thin needle. The Buongiorno nanofluid model is incorporated to model the governing expressions. The flow is conducted electrically and generated through stretching impact. Internal diffusion of particle, homogenous–heterogeneous reactions and radiative heat flux effects are utilized to examine the behavior of heat and mass transport on the surface of thin needle. Suitable similarity variables and boundary layer approximations are used to turn into dimensionless one. After that, numerical out-

*,†Corresponding authors.

comes are computed by a Shooting method (bvp4c) package in MATLAB. The incentives of sundry relevant parameters on the flow field, skin friction coefficient, heat transfer rate, temperature field and concentration distribution are portrayed via graphical tactic and have been elucidated in detail. The outcomes indicate that the temperature distribution is more versus rising values of radiative heat flux, magnetic parameter and Eckert number.

Keywords: Magneto-Cross nanofluid; homogeneous–heterogeneous reactions; radiative heat flux; viscous dissipation; stantion point flow; magnetohydrodynamics (MHD).

PACS numbers: 83.50.Ha, 47.60.Dx

1. Introduction

Due to the significance of different mechanical and industrial applications, the analysis of flow and heat and mass transportations towards a thin moving needle has been inspected by numerous investigators and specialists with various flow constraints. Some of these applications are microscale cooling devices for heat evacuation application, hot wire anemometer and microstructure electronic gadgets which prompt high effectiveness and compactness and so many others. The thin needle term is characterized as a parabolic revolution about its axes direction subject to variable thickness. The movement of the needle occupies from the ambient direction, and this circumstance is the principle anxiety in test analyses (experimental) for the liquid flow and heat and mass transportation investigation so as to measure the temperature, concentration and velocity fields of the system. Numerous researches and investigations concerning nanofluid over a thin needle and also a stretched surface of disk or sheet were carried out by the engineers and mathematicians i.e., Ahmad *et al.*,[1] Trimbitas *et al.*,[2] Hayat *et al.*,[3] Ahmad *et al.*,[4] Bano and Singh,[5] Afridi and Qasim,[6] Khan *et al.*,[7] Waini *et al.*,[8] Hashim *et al.*[9] and Khan *et al.*[10]

As a developing research field, nanofluids have caught massive enthusiasm from analyst and researchers over the globe and have been the important type of escalated research for the last couple of decades. This momentous heat transport medium advances thermal conductivity via suspensions of solid particles and offers a chance of enhanced heat transport for large applications. Nanoliquids have captivating transport characteristics and heat transfer execution as well as tremendous fruitful applications due to which these are a most significant and classical fluids for the next heat generator heat transport. To date, all exploration exercises have been produced due to early exploratory analyses, which estimated abnormally large thermal conductivity augmentation for a small nanoparticles volume fraction. Thermophoresis diffusion and Brownian movement are the two primary factors of the Buongiorno nanofluid model for irregular augmentation of thermal conductivity while utilizing the dualistic liquids like nanoparticles and continuous phase liquid (base fluid). This model provides help to the scientists and mechanical engineers because of its fruitful and meaningful applications in the marvels of science and innovation. Thermophoresis diffusion of particles along with random motion of ma-

terial particles (Brownian moment) helps in germanium dioxide optical fibers and assembling communication engineering silicon. Several researches concerning heat and mass transportation and fluid flow by a stretched curved and flat surfaces of disk or sheet were carried out by the investigators and engineers.[11–28]

The target of the present research communication is to explore the heat and mass transportation and nanofluid flow by a surface of thin moving needle in a parallel free stream of magneto-Cross nanomaterial. The effects of Brownian movement, internal diffusion of particles, thermophoresis and radiative heat flux are also taken into consideration. The total entropy rate is computed by substituting the concentration, temperature and velocity fields obtained from the mass, energy and momentum expressions. The mathematical modeling, schematic flow diagram and governing flow expressions are reported in Sec. 2. The modeling of entropy generation is elaborated in Sec. 3. The pertinent flow parameters and engineering interest such as skin friction coefficient and Nusselt number are discussed in Sec. 4. Finally, the fruitful and meaningful observations of the problem are presented in Sec. 5.

2. Mathematical Formulation

Here, we consider steady, two-dimensional, incompressible nanomaterial flow of magneto-Cross fluid by a stretched surface of thin needle, where the needle moving with velocity $U_w(x)$ and $r = R(x)$ the radius. Also, the Cartesian coordinates r and x, respectively, indicate the radial and axial axes. The flow geometry and the associated coordinate system are shown in Fig. 1.

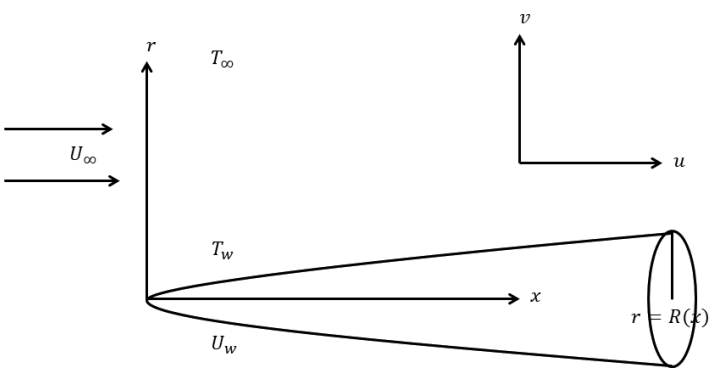

Fig. 1. Flow diagram.

In this case, we consider the following assumptions:

(i) Pressure gradient i.e., $\frac{\partial p}{\partial x}$ is neglected along the surface of needle.
(ii) The needle thickness is smaller comparable to the thermal as well as momentum layer over it.
(iii) In transverse direction, the impact of curvature is prominent.

(iv) The induced magnetic field is ignored due to small Reynolds number.
(v) Both homogeneous–heterogeneous reactions are accounted.

The behavior of flow is examined by considering homogeneous type of reaction at the surface subject to cubic autocatalytic as[2,5,7,8]:

The homogenous reaction in cubic autocatalysis is defined as[12]

$$A^* + 2B* \to 3B^*, \quad \text{rate} = k_c a b^2, \tag{1}$$

and the heterogeneous reaction is

$$A^* \to B^*, \quad \text{rate} = k_s a. \tag{2}$$

Note that k_c and k_s highlight the reaction rate constant and a and b the concentrations of species A^* and B^*.

Under the spirit of aforementioned assumptions, the governing equations of the magneto-Cross nanomaterial, steady, incompressible two-dimensional flow over a thin needle are

$$\frac{\partial}{\partial x}(ru) + \frac{\partial}{\partial r}(rv) = 0, \tag{3}$$

$$u\frac{\partial u}{\partial x}+v\frac{\partial u}{\partial r}=U_\infty \frac{dU_\infty}{dx}+\nu_f\left(\frac{\partial}{\partial r}+\frac{1}{r}\right)\left[\left(\frac{\partial u}{\partial r}\right)\left\{1+\left(\Gamma\left|\frac{\partial u}{\partial r}\right|\right)^n\right\}^{-1}\right]-\frac{\sigma_f B_0^2(u-U_\infty)}{\rho_f}\Bigg\} \tag{4}$$

$$\left.\begin{aligned}\left(u\frac{\partial T}{\partial x}+v\frac{\partial T}{\partial r}\right) &= \frac{k_f}{(\rho c_p)_f}\left(\frac{\partial^2 T}{\partial r^2}+\frac{1}{r}\frac{\partial T}{\partial r}\right)+\frac{\eta_0}{(\rho c_p)_f}\left\{1+\Gamma\left|\frac{\partial u}{\partial r}\right|^n\right\}^{-1}\left(\frac{\partial u}{\partial r}\right)^2\\ &+\frac{16\sigma^*}{3k^*(\rho c_p)_f}\left\{T^3\frac{\partial^2 T}{\partial r^2}+3T^2\left(\frac{\partial T}{\partial r}\right)^2\right\}\\ &+\frac{(\rho c_p)_p}{(\rho c_p)_f}\left[D_B\frac{\partial a}{\partial r}\frac{\partial T}{\partial r}+D_B\frac{\partial b}{\partial r}\frac{\partial T}{\partial r}+\frac{D_T}{T_\infty}\left(\frac{\partial T}{\partial r}\right)^2\right]+\frac{\sigma_f B_0^2 u^2}{(\rho c_p)_f},\end{aligned}\right\} \tag{5}$$

$$\left(u\frac{\partial a}{\partial x}+v\frac{\partial a}{\partial r}\right)=\frac{D_A}{r}\frac{\partial}{\partial r}\left(r\frac{\partial a}{\partial r}\right)+\frac{D_T}{T_\infty}\frac{1}{r}\frac{\partial}{\partial r}\left(r\frac{\partial T}{\partial r}\right)-k_c a b^2, \tag{6}$$

$$\left(u\frac{\partial b}{\partial x}+v\frac{\partial b}{\partial r}\right)=\frac{D_B}{r}\frac{\partial}{\partial r}\left(r\frac{\partial b}{\partial r}\right)+\frac{D_T}{T_\infty}\frac{1}{r}\frac{\partial}{\partial r}\left(r\frac{\partial T}{\partial r}\right)+k_c a b^2, \tag{7}$$

with

$$\left.\begin{aligned}u = U_w(x), \quad v = 0, \quad T = T_w, \quad D_A\frac{\partial a}{\partial r} = k_s a, \quad D_B\frac{\partial b}{\partial r} = -k_s a, \quad \text{at } r = R(x)\\ u \to U_\infty(x), \quad T \to T_\infty, \quad a \to a_0, \quad b \to 0 \quad \text{as } r \to \infty.\end{aligned}\right\} \tag{8}$$

Note that η_0 highlights zero shear-rate viscosity, u, v velocity components, U_w stretching velocity, x, r coordinates system, U_∞ free stream velocity, ν_f kinematic viscosity, σ_f electrical conductivity, n power law index, B_0 magnetic field strength, ρ_f density, Γ material time constant, T temperature, k_f thermal conductivity, $(\rho c_p)_p$ and $(\rho c_p)_f$, respectively, heat capacity of nanoparticles and fluid, σ^* Stefan–Boltzmann constant, D_T thermophoresis coefficient, k^* mean absorption coefficient, D_B Brownian movement coefficient, T_∞ ambient temperature and T_w wall temperature.

Let us consider the following variables leading to dimensionless flow expressions:

$$\begin{aligned} u = 2Uf'(\eta), \quad v = -\frac{\nu_f}{r}f + \eta\frac{\nu_f}{r}f'(\eta), \quad \eta = \frac{Ur^2}{\nu_f x}, \\ \theta(\eta) = \frac{T - T_\infty}{T_w - T_\infty}, \quad \phi(\eta) = \frac{a_1}{a_0}, \quad \chi(\eta) = \frac{a_2}{a_0}. \end{aligned} \tag{9}$$

The continuity equation is identically satisfied in view of Eq. (9). Also, $U = U_w + U_\infty \neq 0$ signifies the composite velocity and $f(\eta), \theta(\eta), \phi(\eta), \chi(\eta)$ represent the dimensionless velocity, temperature and concentrations fields. Let $\eta = A$ in Eq. (6), we arrive $R(x) = (\frac{\text{Avx}}{U})^{1/2}$ (prescribes the shape and size of the surface of revolution).

As

$$T = T_\infty[1 + (\theta_f - 1)\theta], \tag{10}$$

where θ_f $(= \frac{T_w}{T_\infty} > 1)$ symbolizes the temperature ratio variable.

After implementing Eq. (9), we arrive

$$\text{Re}[1 + (1-n)(4\text{We}f'')^n]f''' + \frac{1}{2}[1 + (4\text{We}f'')^n]^2\left\{ff'' - \frac{1}{8}M(2f' - \lambda)\right\} = 0, \tag{11}$$

$$\left.\begin{aligned} &\theta' + \eta\theta'' + \frac{1}{2}\Pr f\theta' + \frac{4}{3\text{Nr}}\left\{\begin{aligned}&[1 + (\theta_f - 1)\theta]^3\left(\frac{1}{2}\theta' + \eta\theta''\right) \\ &+ 3\eta[1 + (\theta_f - 1)\theta]^2(\theta_f - 1)(\theta')^2\end{aligned}\right\} \\ &+ 4\eta\Pr\text{Ec}\left[\frac{(f'')^2}{1 + (4\text{We}f'')^n}\right] + \eta\Pr[\text{Nb}(\theta'\phi' + \theta'\chi') + \text{Nt}(\theta')^2] \\ &+ \Pr\text{Ec}M(f')^2 = 0, \end{aligned}\right\} \tag{12}$$

$$\eta\phi'' + 2\phi' + \text{Sc}f'\phi' + 2\left(\frac{\text{Nt}}{\text{Nb}}\right)(\theta' + \eta\theta'') - \frac{1}{2}\text{Sc}K_1\phi\chi^2 = 0, \tag{13}$$

$$\Omega\eta\chi'' + 2\chi' + \text{Sc}f'\chi' + 2\left(\frac{\text{Nt}}{\text{Nb}}\right)(\theta' + \eta\theta'') + \frac{1}{2}ScK_1\phi\chi^2 = 0, \tag{14}$$

with

$$\left.\begin{aligned} f'(A) = \frac{1}{2}(1-\lambda),\ f(A) = 0,\ \theta(A) = 1,\ \varphi'(A) = K_2\varphi,\ \Omega\chi'(A) = -\frac{1}{2}K_2\varphi \text{ at } \eta = A, \\ f'(\infty) \to \tfrac{1}{2}\lambda, \quad \theta(\infty) \to 0, \quad \varphi(\infty) \to 1, \quad \chi(\infty) \to 0 \quad \text{as } \eta \to \infty. \end{aligned}\right\} \tag{15}$$

Now, utilizing the concept of equal diffusion coefficients i.e., $D_A = D_B = 1$, or $\Omega = 1$. This assumption develops the following relation:

$$\phi(\eta) + \chi(\eta) = 1. \tag{16}$$

Under the above assumptions, Eqs. (12)–(15) take the form

$$\left.\begin{aligned} &\theta' + \eta\theta'' + \frac{1}{2}\Pr f\theta' + \frac{4}{3N_R}\left\{\begin{aligned}&[1+(\theta_f-1)\theta]^3\left(\frac{1}{2}\theta' + \eta\theta''\right)\\ &+3\eta[1+(\theta_f-1)\theta]^2(\theta_f-1)(\theta')^2\end{aligned}\right\}\\ &+4\eta\Pr\mathrm{Ec}\left[\frac{(f'')^2}{1+(4\mathrm{We}f'')^n}\right] + \eta\Pr\mathrm{Nt}(\theta')^2 + \Pr\mathrm{Ec}M(f')^2 = 0, \end{aligned}\right\} \tag{17}$$

$$\eta\phi'' + 2\phi' + \mathrm{Sc}f'\phi' + 2\left(\frac{\mathrm{Nt}}{\mathrm{Nb}}\right)(\theta' + \eta\theta'') - \frac{1}{2}\mathrm{Sc}K_1\phi(1-\phi)^2 = 0, \tag{18}$$

$$\left.\begin{aligned} &f'(A) = \frac{1}{2}\lambda, \quad f(A) = 0, \quad \theta(A) = 1, \quad \phi'(A) = -\frac{1}{2}K_2\phi(A) \quad \text{at } \eta = A,\\ &f'(\infty) \to \frac{1}{2}(1-\lambda), \quad \theta(\infty) \to 0, \quad \phi(\infty) \to 1 \quad \text{as } \eta \to \infty. \end{aligned}\right\} \tag{19}$$

The dimensionless variables appearing in the above equations are as follows:

$$\left.\begin{aligned} &\mathrm{We} = \frac{\lambda U\mathrm{Re}}{x}, \quad \mathrm{Re} = \frac{Ur}{\nu_f}, \quad M = \frac{\sigma_f B_0^2 x}{\rho_f U}, \quad \Omega = \frac{D_B}{D_A}, \quad \lambda = \frac{U_w}{U},\\ &\mathrm{Nr} = \frac{k_f k^*}{4\sigma^* T_\infty}, \quad \mathrm{Nt} = \frac{\tau D_T T_\infty(\theta_f - 1)}{\nu_f T_\infty}, \quad K_1 = \frac{k_c C_0^2 x}{U}, \quad K_2 = \frac{k_s \nu_f x}{D_A U r},\\ &\Pr = \frac{\nu_f}{\alpha_f}, \quad \mathrm{Sc} = \frac{\nu_f}{D}, \quad \mathrm{Nb} = \frac{\tau D_B a_0}{\upsilon}, \quad E_c = \frac{U^2}{(c_p)_f(\theta_f - 1)T_\infty}, \quad \theta_f = \frac{T_w}{T_\infty}. \end{aligned}\right\} \tag{20}$$

Here, We indicates Weissenberg parameter, Re Reynolds number, M Hartmann number, Ω ratio of diffusion coefficients, Pr Prandtl number, Sc Schmidt number, Nr radiation parameter, Nt thermophoresis parameter, λ ratio parameter, K_1 homogeneous reaction parameter, Nb Brownian motion parameter, K_2 heterogeneous reaction parameter, Ec Eckert number and θ_f temperature ratio parameter.

The dimensionless form of skin friction coefficient and Nusselt number is addressed as

$$\mathrm{Re}^{\frac{1}{2}} C_f = 8A^{\frac{1}{2}} \frac{f''(A)}{1 + \mathrm{We}|f''(A)|^n}, \tag{21}$$

$$\mathrm{Re}^{-\frac{1}{2}}\mathrm{Nu} = -\left[1 + \frac{4}{3}\mathrm{Nr}\{\theta(A)(\theta_w - 1) + 1\}^3\right]\theta'(A). \tag{22}$$

3. Entropy Generation

In this study, viscous dissipation, nonlinear radiative heat flux, mass transfer and Ohmic heating effects are taken into account on entropy generation minimization. The local entropy generations (EG) is given by[6,7]

$$\left.\begin{aligned}\dot{S}'''_{\text{gen}} = &\underbrace{\frac{k_f}{T^2}\left[\left(\frac{\partial T}{\partial r}\right)^2\right] + \frac{k_f}{T^2}\left[\frac{16\sigma^* T^3}{3k^* k_f}\left(\frac{\partial T}{\partial r}\right)^2\right]}_{\text{Heat transfer irreversibility}} \\ &+ \underbrace{\frac{\eta_0}{T}\left\{\frac{(\frac{\partial u}{\partial r})^2}{1+\lambda|\frac{\partial u}{\partial r}|^n}\right\}}_{\text{Viscous dissipation irreversibility}} + \underbrace{\frac{\sigma_f B_0^2 u^2}{T}}_{\text{Joule heating irreversibility}} \\ &+ \underbrace{\frac{R^* D_A}{T}\left(\frac{\partial a}{\partial r}\frac{\partial T}{\partial r}\right) + \frac{R^* D_A}{a}\left\{\left(\frac{\partial a}{\partial r}\right)^2\right\} + \frac{R^* D_B}{b}\left\{\left(\frac{\partial b}{\partial r}\right)^2\right\} + \frac{R^* D_B}{T}\left(\frac{\partial b}{\partial r}\frac{\partial T}{\partial r}\right)}_{\text{Mass transfer irreversibility}}\end{aligned}\right\}. \tag{23}$$

The entropy generation number (EGN) is the dimensionless form of entropy generation rate (EGR) which highlights the relation between actual EGR which is denoted by ($\dot{S}'''_{\text{gen}}$) and characteristic EGR which is denoted by ($\dot{S}'''_0$). In Eq. (23), R^* indicates molar gas constant.

Implementing Eq. (9), the dimensionless form is

$$\left.\begin{aligned}N_G &= \frac{S'''_{\text{gen}}}{S'''_0} \\ &= \text{Re}^2\left\{1+\frac{4}{3}\text{Nr}[1+(\theta_f-1)\theta]^3\right\}\frac{(\theta')^2}{[1+(\theta_f-1)\theta]^2} \\ &\quad + \frac{16\text{Br}}{(\theta_f-1)[1+(\theta_f-1)\theta]}\left\{\frac{(f'')^2}{1+(4\text{We}\,f'')^n}\right\} \\ &\quad + \frac{4M\text{Br}\,\text{Re}}{(\theta_f-1)[1+(\theta_f-1)\theta]}(f'')^2 + \frac{4\Omega_1\text{Re}^2}{(\theta_f-1)}\phi'\left(\theta'+\frac{\phi'}{\phi}\right) \\ &\quad + \frac{4\Omega_2\text{Re}^2}{(1-\phi)}(\phi')^2 - \frac{4\Omega_2\text{Re}^2}{(\theta_f-1)[1+(\theta_f-1)\theta]}\theta'\phi',\end{aligned}\right\} \tag{24}$$

where $\text{Re} = \frac{\rho_f x U}{\eta_0}$ indicates Reynolds number, $Br = \frac{\eta_0 U^2}{k_f T_\infty(\theta_f-1)}$ is the Brinkman number, $\Omega_1 = \frac{R^* D_A a_0}{k_f}$ is the diffusion rate for homogeneous reaction, $\Omega_2 = \frac{R^* D_B a_0}{k_f}$ is the diffusion rate for heterogeneous reaction and $S'''_0 = \frac{k_f(T_w-T_\infty)^2}{T_\infty^2 x^2}$ nondimensional characteristic EGR.

The Bejan number is the ratio of EG via heat transfer plus that due to nanoparticle mass transfer to the total EG. The Bejan number for the stated flow problem

is addressed as

$$\mathrm{Be} = \frac{\left.\begin{array}{l} \mathrm{Re}^2\left\{1+\frac{4}{3}\mathrm{Nr}[1+(\theta_f-1)\theta]^3\right\}\frac{(\theta')^2}{[1+(\theta_f-1)\theta]^2}+\frac{4\Omega_1\mathrm{Re}^2}{(\theta_f-1)}\phi'\left(\theta'+\frac{\phi'}{\phi}\right) \\ +\frac{4\Omega_2\mathrm{Re}^2}{(1-\phi)}(\phi')^2-\frac{4\Omega_2\mathrm{Re}^2}{(\theta_f-1)[1+(\theta_f-1)\theta]}\theta'\phi' \end{array}\right\}}{\left.\begin{array}{l} \mathrm{Re}^2\left\{1+\frac{4}{3}\mathrm{Nr}[1+(\theta_f-1)\theta]^3\right\}\frac{(\theta')^2}{[1+(\theta_f-1)\theta]^2} \\ +\frac{16\mathrm{Br}}{(\theta_f-1)[1+(\theta_f-1)\theta]}\left\{\frac{(f'')^2}{1+(4\mathrm{We}\,f'')^n}\right\} \\ +\frac{4M\,\mathrm{Br}\,\mathrm{Re}}{(\theta_f-1)[1+(\theta_f-1)\theta]}(f'')^2+\frac{4\Omega_1\mathrm{Re}^2}{(\theta_f-1)}\phi'\left(\theta'+\frac{\phi'}{\phi}\right) \\ +\frac{4\Omega_2\mathrm{Re}^2}{(1-\phi)}(\phi')^2-\frac{4\Omega_2\mathrm{Re}^2}{(\theta_f-1)[1+(\theta_f-1)\theta]}\theta'\phi' \end{array}\right\}}. \quad (25)$$

4. Results

For solution development of the nonlinear flow expressions i.e., (11), (12) and (18) subjected to boundary constraint (19), we implemented the Shooting method (bvp4c) package in MATLAB. Figure 1 is portrayed for the schematic flow analysis and Figs. 2–10 and Tables 1 and 2 are revealed for elaboration of important flow parameters against velocity field $f'(\eta)$, temperature field $\theta(\eta)$ skin friction coefficient $\mathrm{Re}^{\frac{1}{2}}C_f$ concentration field $\phi(\eta)$ and Nusselt number $\mathrm{Re}^{-\frac{1}{2}}\mathrm{Nu}$. The numerical results of $\mathrm{Re}^{\frac{1}{2}}C_f$ against magnetic parameter ($M = 0.00, 0.03, 0.06, 0.09$) and

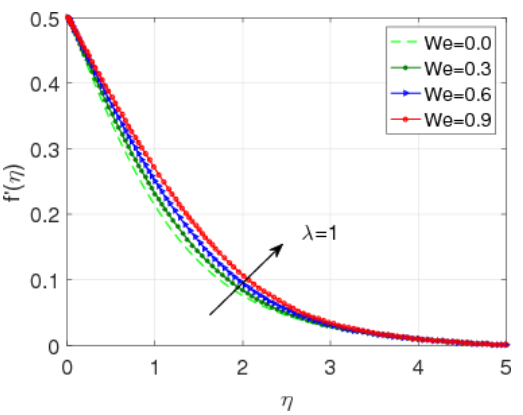

Fig. 2. (Color online) $f'(\eta)$ versus parameter We.

Weissenberg number ($We = 0.0, 0.3, 0.6, 0.9$) are portrayed in Table 1. Here, we can observe that the magnitude of skin friction coefficient decreases versus rising estimations of magnetic parameter as well as Weissenberg number. The physical impact of important factor of this flow i.e., Nusselt number or heat transfer rate ($\mathrm{Re}^{-\frac{1}{2}}\mathrm{Nu}$) is numerically calculated and discussed subject to radiative parameter ($Nr = 0.1, 0.2, 0.3, 0.4$) and Eckert number ($Ec = 0.01, 0.03, 0.05, 0.07$) in Table 2. As expected, the magnitude of Nusselt number or heat transfer rate gradually declines as we increase the range of radiative parameter and Eckert number.

Figure 2 portrays Weissenberg number ($We = 0.0, 0.3, 0.6, 0.9$) inspiration against $f'(\eta)$. Clearly, velocity field specifies increasing trend when Weissenberg number is increased. Physically, the resistive effects inside the working fluid is diminished versus rising Weissenberg number. Figure 3 interprets power index ($n = 1, 2, 3, 4$) contribution on velocity field. This Fig. 3, witness velocity field increment. Figure 4 reports Reynolds number ($\mathrm{Re} = 0.1, 0.15, 0.2, 0.25$) impact on velocity field. Since, Reynolds number is the ratio of inertial forces to the viscous and here for rising values of Reynolds number, the viscous forces decreases and as a results less resistive force face by the material particles. That is why the velocity field increases. The variations of Eckert number ($Ec = 0.01, 0.03, 0.05, 0.07$) against thermal field are indicated in Fig. 5. Figure 5 acknowledges an increase in both thermal field as well as thermal layer thickness versus larger Eckert number. In physical point of view, larger Eckert provides heat to the working fluid and consequently the temperature of the fluid particles increases. Figure 6 plots temperature distribution for radiative heat flux parameter ($Nr = 0.1, 0.2, 0.3, 0.4$). Here, thermal field is found rising function of larger radiative heat parameter. Physically, extra heat amount is transferred when radiative heat parameter is upsurge and thus the temperature distribution rises. The salient characteristics of thermophoresis diffusion ($Nt = 0.1, 0.2, 0.3, 0.4$) and Brownian motion ($Nb = 0.13, 0.15, 0.17, 0.19$) on the temperature and concentration fields, respectively, are illustrated graphically in Figs. 7 and 9. Here, contrast influence on the thermal field as well as concentration field is noticed against larger values of thermophoresis diffusion and Brownian diffusion parameter, respectively. In Fig. 7, the thermal field and its thermal layer thickness boosts versus higher estimations of thermophoretic diffusion parameter, while concentration field and associated layer thickness decays against Brownian diffusion parameter (see Fig. 9). Figure 8 divulges the liquid concentration field for distinct estimations of Schmidt number ($Sc = 0.1, 0.2, 0.3, 0.4$) at the other pertinent fluid parameters fixed. Here, concentration field is a diminishing function of Schmidt number. Since the Schmidt number is the combination of kinematic viscosity and molecular diffusion i.e., $Sc = \frac{\nu}{D}$, it is utilized to illustrate liquid flows in which there are concurrent momentum as well as mass diffusion convection processes. Figure 10 highlights the salient attributes of thermophoretic variable on the concentration field. Here, both solutal field and solutal layer thickness increase against higher values of thermophoretic parameter.

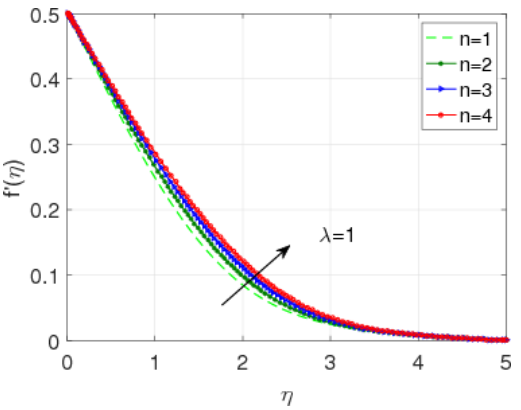

Fig. 3. (Color online) $f'(\eta)$ versus parameter n.

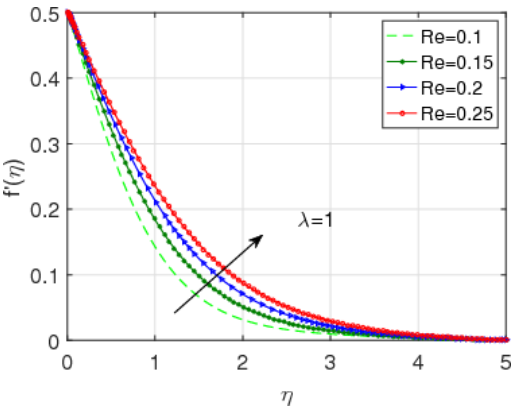

Fig. 4. (Color online) $f'(\eta)$ versus parameter Re.

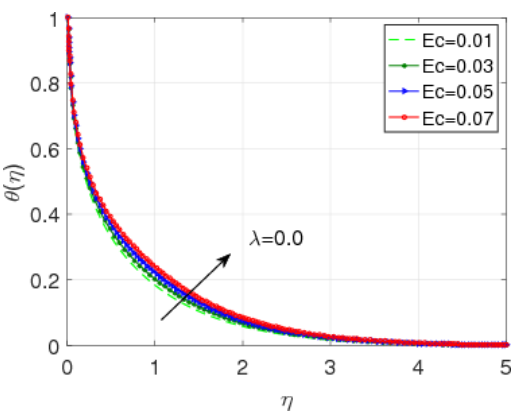

Fig. 5. (Color online) $\theta(\eta)$ versus parameter Ec.

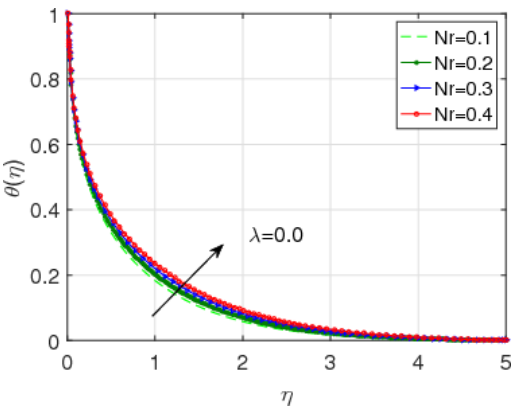

Fig. 6. (Color online) $\theta(\eta)$ versus parameter Nr.

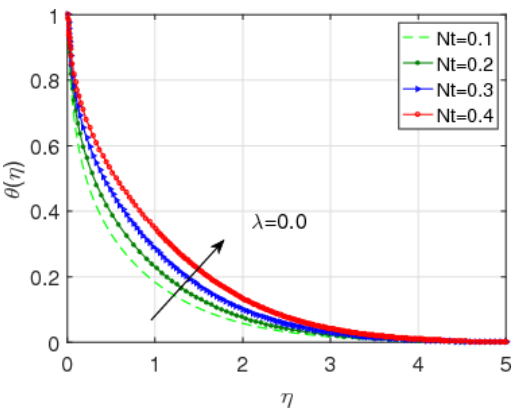

Fig. 7. (Color online) $\theta(\eta)$ versus parameter Nt.

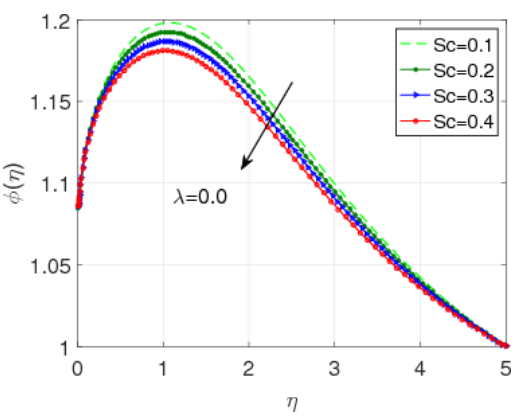

Fig. 8. (Color online) $\phi(\eta)$ versus parameter Sc.

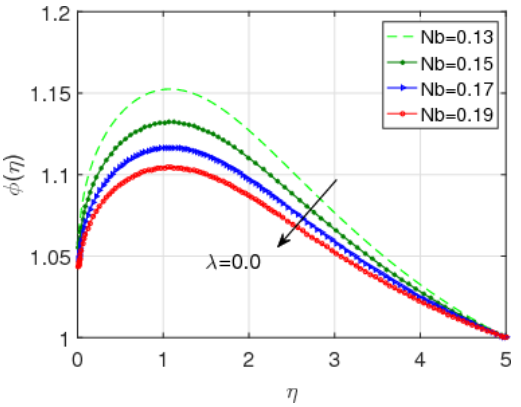

Fig. 9. (Color online) $\phi(\eta)$ versus parameter Nb.

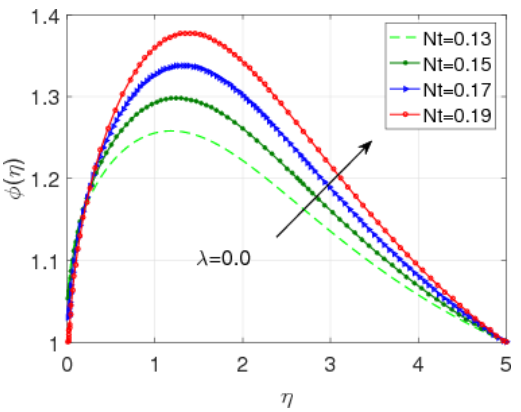

Fig. 10. (Color online) $\phi(\eta)$ versus parameter Nt.

Table 1. Characteristics of skin friction coefficient versus magnetic parameter and Weissenberg number.

M	We	f''
0.0		−0.769389
0.03		−0.748534
0.06		−0.728942
0.09		−0.710402
	0.0	−0.983996
	0.3	−0.748534
	0.6	−0.593679
	0.9	−0.47911

Table 2. Characteristics of Nusselt number versus radiative heat flux and Eckert number.

Nr	Ec	$-\theta'$
0.1		14.0896
0.2		13.6925
0.3		13.3497
0.4		13.0494
	0.01	14.0896
	0.03	13.7252
	0.05	13.3496
	0.07	12.9624

5. Conclusion

This research communication concerns the analysis of electrically conducting magnetized stagnation point flow, heat and mass transport of non-Newtonian fluid (Cross fluid) over a stretched moving surface of thin needle. The Buongiorno nanofluid model is incorporated to model the governing expressions. The flow is conducting electrically and generated through stretching impact. Internal diffusion of particle, homogenous–heterogeneous reactions and radiative heat flux effects are utilized to examine the behavior of heat and mass transport on the surface of thin needle. Suitable similarity variables and boundary layer approximations are used to turn into dimensionless one. After that, numerical outcomes are computed by a Shooting method (bvp4c) package in MATLAB. We have the following fruitful and noteworthy points from the aforementioned flow problem:

- Rising Weissenberg number corresponds to larger velocity field.
- An enhancement in power law index, the velocity field is increased.
- An increament in radiative heat parameter and Eckert number yield thermal field augmentation.
- There is a degeneration in concentration field versus Schmidt number and Brownian motion parameter.
- Both skin friction coefficient and Nusselt number are diminished for rising estimations of magnetic parameter, Weissenberg number, radiative parameter and Eckert number.

Acknowledgments

The research was supported by the National Natural Science Foundation of China (Grant Nos. 11971142, 11871202, 61673169, 11701176, 11626101 and 11601485).

References

1. S. Ahmad *et al.*, *Int. Commun. Heat Mass Transf.* **35**, 157 (2008).
2. R. Trimbitas, T. Grosan and I. Pop, *Int. J. Numer. Methods Heat Fluid Flow* **24**, 579 (2014).

3. T. Hayat *et al.*, *J. Mol. Liq.* **224**, 786 (2016).
4. R. Ahmad, M. Mustafa and S. Hina, *Chin. J. Phys.* **55**, 1264 (2017).
5. N. Bano and B. B. Singh, *Int. Commun. Heat Mass Transf.* **84**, 41 (2017).
6. M. I. Afridi and M. Qasim, *Int. J. Thermal Sci.* **123**, 117 (2018).
7. M. W. A. Khan *et al.*, *Phys. B: Condens. Matter* **534**, 113 (2018).
8. I. Waini, A. Ishak and I. Pop, *Chin. J. Phys.* **60**, 651 (2019).
9. Hashim, A. Hamid and M. Khan, *Chin. J. Phys.* **64**, 227 (2020).
10. U. Khan *et al.*, *J. Mater. Res. Technol.* **9**, 3817 (2020).
11. N. Acharya, K. Das and P. K. Kundu, *Appl. Nanosci.* **8**, 369 (2018).
12. M. I. Khan *et al.*, *J. Colloid Interface Sci.* **498**, 85 (2017).
13. J. Prakash, D. Tripathi and O. A. Bég, *Appl. Nanosci.* **10**, 1693 (2020).
14. M. I. Khan *et al.*, *J. Magn.* **25**, 8 (2020).
15. W. Jamshed and A. Aziz, *Appl. Nanosci.* **8**, 685 (2018).
16. M. I. Khan *et al.*, *Arab. J. Sci. Eng.* **45**, 4939 (2020).
17. I. Khan *et al.*, *Appl. Nanosci.* **10**, 1521 (2020).
18. S. Z. Abbas *et al.*, *Comput. Methods Programs Biomed.* **190**, 105363 (2020).
19. R. Muhammad *et al.*, *Comput. Methods Programs Biomed.* **189**, 105294 (2020).
20. S. Ahmad *et al.*, *Int. J. Mod. Phys. B* **34**, 2050130 (2020).
21. R. Muhammad *et al.*, *Comput. Methods Programs Biomed.* **188**, 105298 (2020).
22. M. I. Khan and F. Alzahrani, *Int. J. Mod. Phys. B* **34**, 2050132 (2020).
23. M. K. Nayak *et al.*, *J. Mater. Res. Technol.* **9**, 7387 (2020).
24. H. J. Xu *et al.*, *Chem. Eng. Sci.* **195**, 462 (2019).
25. M. I. Khan, F. Alzahrani and A. Hobiny, *Alex. Eng. J.* **59**, 1761 (2020).
26. H. Xu, Z. Xing and K. Vafai, *Int. J. Heat Fluid Flow* **77**, 242 (2019).
27. M. I. Khan and F. Alzahrani, *J. Theor. Comput. Chem.* **19**, 2040006 (2020).
28. H. Xu, Z. Xing and A. Ghahremannezhad, *J. Porous Media* **22**, 1553 (2019).